Mechanism and Machine Theory 219 (2026) 106320

Contents lists available at ScienceDirect

Mechanism and Machine Theory

journal homepage: www.elsevier.com/locate/mechmt

Research paper

Synthesis at the output port of compliant mechanisms through the instantaneous geometric invariants

M. Verotti

Department of Mechanical, Energy, Management and Transportation Engineering, University of Genova, Via all'Opera Pia, 15 - 16145, Genoa, Italy

ARTICLE INFO

Keywords:
Compliant mechanisms design
Compliant mechanisms synthesis
Flexures
Instantaneous geometric invariants
Kinematics

ABSTRACT

Recently, the instantaneous geometric invariants have proved to be a fundamental tool for the analysis of the motion generated by flexure hinges. In this paper, the invariants are applied to the synthesis of compliant mechanisms at the output port level. The motion of the moving plane associated to the output port is described through fundamental geometric entities, that are the inflection circle, the cubic of stationary curvature, and its derivative. The proposed synthesis procedure aims to reshape the output port to embody the special points on the plane, that are the Ball's and the Burmester's points, approximating straight and circular paths to the third and to the fourth order, respectively. The method is implemented for the design of a compliant mechanism and numerical simulations are conducted to verify the theoretical results. A discussion of the advantages and disadvantages of the method is presented.

1. Introduction

Due to their advantages over the traditional rigid-body systems, compliant mechanisms are being increasingly implemented in many industrial and research fields, as robotics [1–3], precision engineering [4–6], aerospace [7–9], and micro-electromechanical systems [10–13]. In accordance with this trend, many investigations have been presented in the literature, proposing analysis and modeling methods both at the flexure level [14–16] and at the mechanism level [17–19].

Numerous studies have also focused on the synthesis aspect, developing advanced procedures to overcome the intrinsic challenges of compliant systems, that are kinematics and statics coupling, geometric nonlinearities, and complex topologies. Generally, the methods presented in Literature propose a synthesis *at the mechanism level*, aiming to delineate an elastic suspension, that is a compliant structure with lumped or distributed compliance, able to meet assigned design requirements under specific constraints. These methods can be classified in topology optimization, kinematics-based, building block [20,21], and projective [22–24] approaches.

Topology optimization seeks the optimal material layout in the design space that meets the assigned requirements, in terms of objective functions and constraints. Material properties and element density are some of the possible variables in the algorithm models. Discrete or continuum parametrizations can be implemented in the procedure [25–27].

Topology-optimization approaches have been employed for the design of fully, partially, and contact-aided compliant mechanisms [28–31]. Beyond structural performance, such strategies have further been used for path generation, where the topology or geometry is modified to obtain precise paths for prescribed points [32–34].

Kinematics-based approaches comprise the rigid-body replacement and the freedom and constraint topology. Starting from a rigid-body mechanism layout, the rigid-body-replacement method consists of designing a compliant mechanism by replacing the traditional kinematic pairs with flexure hinges. This step is usually performed by resorting to a pseudo-rigid body model, which relates the

E-mail address: matteo.verotti@unige.it

https://doi.org/10.1016/j.mechmachtheory.2025.106320
Received 8 November 2025; Received in revised form 8 December 2025; Accepted 8 December 2025
Available online 17 December 2025

load-displacement relation of the rigid and of the elastic mechanisms. Several pseudo-rigid body models can be considered, characterized by different numbers of degrees of freedom [35,36] or determined according to different kinematic criteria [37,38]. The freedom and constraint topology approach proposes a library of vector spaces, derived from screw theory, projective geometry, and exact-constraint design, for defining a compliant mechanism with specified mobility [39,40]. This method has been applied in the design of systems with different topologies [41,42] and to compliant transmission mechanisms [43].

The building block method defines the compliant mechanism as a network of compliant structures described by the load-displacement relations between the input and output ports [44,45]. Recently, the geometry of concatenation has been described through several design rules developed from the relations between eigentwists and eigenwrenches [46]. According to the compliant building elements approach, the quantitative information of a compliant system have been encoded in a parametric matrix, and a library of compliant elements was presented to generate the initial stage topological designs [47].

A geometric framework based on projective geometry, in particular on the antipolarity transformation between poles of displacements and lines of action, led to the description of the load-displacement relation in terms of the ellipse of elasticity [48,49].

As previously mentioned, the methods described above focus on the mechanism level, defining the elastic suspension according to requirements usually formulated in terms of degrees of freedom or constraint, and of compliance or stiffness directions. However, the synthesis problem can be addressed from another standpoint, *at the output port level.* In fact, a compliant mechanism can be seen as a two-port system, consisting of an elastic suspension connecting a moving body to the fixed frame. The output port is the moving body subject to the design requirements, expressed in terms of motion laws or load-displacement relations. The *output port synthesis* aims to meet the functional requirements with an already defined compliant structure, by exploiting the field of displacements of the moving body. An example of application of this approach is the point compliance synthesis method presented in Ref. [23,24]. The points of the moving body have been characterized through the spectral analysis of their corresponding compliance matrix. The synthesis problem has been reduced to a normalized geometric problem formulated as an algebraic system with closed-form solutions.

Recent investigations resorted to the instantaneous geometric invariants for the analysis of flexure hinges with variable cross-section, initial curvature, or subject to combined loads [50–52]. In particular, they have been exploited for the study of the high-order kinematics of constant-curvature flexures [53]. As fundamental tools in the design of rigid-body mechanisms, the invariants were introduced by Krause [54] and developed by Veldkamp, Bottema, and Roth [55,56]. Recently, they have been considered for the description of the kinematics of the hyperbolic plane [57], for the computation of generalized Burmester's points [58,59], and for the determination of the high-order centrodes and Bresse's circles of slider-crank mechanisms [60,61]. With respect to classical motion generation methods based on the kinematic fields of rigid bodies, the proposed synthesis operates on the displacement field resulting from the deformations of an elastic suspension.

In this paper, the geometric invariants are applied to the synthesis of compliant mechanisms at the output port level. Given an assigned elastic suspension, the motion of the moving plane is described through the inflection circle, the cubic of stationary curvature, and its derivative. Then, the output port is specifically modeled to include the special points on the plane that approximate straight and circular paths to the third and to the fourth order, respectively. This study constitutes, to the best of the author knowledge, the first application of instantaneous geometric invariants, up to fourth order, to the synthesis of compliant mechanisms.

The manuscript is organized as follows. In Section 2, the kinematic background is introduced. The motions at the element and at the mechanism level are described in Sections 3 and 4, respectively. The synthesis procedure is detailed in Section 5 and implemented, for the design of a compliant four-bar mechanism, in Section 6. The advantages and disadvantages of the method are discussed in Section 7. Conclusions are reported in Section 8.

2. Instantaneous geometric invariants

With reference to Fig. 1, the reference frames $\mathcal{F} = \{O, X, Y\}$ and $\leq = \{o, x, y\}$ represent the fixed and the moving plane, respectively. The motion of a point P of the moving plane with respect to the fixed reference can be described by

$$\begin{aligned} X(t) &= X_o(t) + x\cos(\phi(t)) - y\sin(\phi(t)), \\ Y(t) &= Y_o(t) + x\sin(\phi(t)) + y\cos(\phi(t)), \end{aligned} \tag{1}$$

where X_o, Y_o, and ϕ are real functions of the time t, and (x, y) are the coordinates of P in $\leq$, not dependent on t. By assuming $d\phi/dt = 1$ and $\phi = 0$ for $t = 0$, $\phi = t$ becomes the independent variable, and X_o and Y_o become function of ϕ. The generic value of ϕ represents one pose of the mobile plane with respect to the fixed one, and Eq. (1) can be rewritten as

$$X = X_o + x\cos\phi - y\sin\phi, \tag{2}$$

$$Y = Y_o + x\sin\phi + y\cos\phi. \tag{3}$$

The previous equations provide a geometry-based description of the motion, useful for the analysis of the motion properties that do not depend on time. The first derivatives of Eq. (3) read

$$X^{(1)} = X_o^{(1)} - x\sin\phi - y\cos\phi, \tag{4}$$

$$Y^{(1)} = Y_o^{(1)} + x\cos\phi - y\sin\phi. \tag{5}$$

By making use of Eq. (3) and Section 2, the equations of the fixed centrode λ can be easily obtained as

$$\lambda_X = X_{P_1} = X_o - Y_o^{(1)}, \tag{6}$$

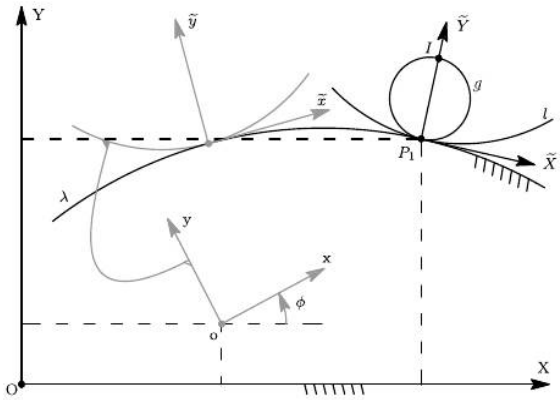

Fig. 1. Reference frames and nomenclature.

$$\lambda_Y = Y_{P_1} = Y_o + X_o^{(1)}. \tag{7}$$

Eq. (7) represent, in $\mathcal{F}$, the loci of the instantaneous center of rotation P_1 during the motion of the moving plane defined by the variable ϕ. The loci of P_1 in the moving reference frame $\leq$ can be obtained as

$$l_x = x_{P_1} = X_o^{(1)} \sin\phi - Y_o^{(1)} \cos\phi, \tag{8}$$

$$l_x = y_{P_1} = Y_o^{(1)} \sin\phi + X_o^{(1)} \cos\phi. \tag{9}$$

Knowing the centrodes and the position of P_1 at $\phi = 0$, the description of the motion can be formulated by introducing two canonical reference frames. The fixed canonical frame, $\widetilde{\mathcal{F}} = \{P_1 \widetilde{X} \widetilde{Y}\}$, associated to the fixed centrode λ, has origin in the instantaneous center of rotation P_1 and $\widetilde{X}$-axis tangent to the centrodes in P_1. The moving canonical frame, $\widetilde{\leq} = \{P_1 \widetilde{x}\widetilde{y}\}$, associated to the moving centrode l, is coincident to $\widetilde{\mathcal{F}}$ at $\phi = 0$.

The instantaneous geometric invariants are defined as

$$a_n = \frac{d^{(n)} \widetilde{X}_{P_1}}{d\phi^n}, \qquad b_n = \frac{d^{(n)} \widetilde{Y}_{P_1}}{d\phi^n}, \tag{10}$$

namely the n-order derivatives of the coordinates $\widetilde{X}_{P_1}$ and $\widetilde{Y}_{P_1}$ of the instantaneous center of rotation P_1 with respect to the independent variable ϕ. Considering the reference configuration ($\phi = 0$), and by introducing the notation

$$X_o^{(n)} = \frac{d^{(n)} X_o}{d\phi^n}, \qquad Y_o^{(n)} = \frac{d^{(n)} Y_o}{d\phi^n}, \tag{11}$$

the invariants can be written as

$$a_0 = b_0 = a_1 = b_1 = a_2 = 0, \tag{12}$$

$$b_2 = \sqrt{\left(X_o^{(2)} + Y_o^{(1)}\right)^2 + \left(Y_o^{(2)} - X_o^{(1)}\right)^2}, \tag{13}$$

$$a_3 = \frac{1}{b_2}\left(\left(X_o^{(3)} + X_o^{(1)}\right)\left(Y_o^{(2)} - X_o^{(1)}\right) - \left(Y_o^{(3)} + Y_o^{(1)}\right)\left(X_o^{(2)} + Y_o^{(1)}\right)\right), \tag{14}$$

$$b_3 = \frac{1}{b_2}\left(\left(X_o^{(3)} + X_o^{(1)}\right)\left(X_o^{(2)} + Y_o^{(1)}\right) + \left(Y_o^{(3)} + Y_o^{(1)}\right)\left(Y_o^{(2)} - X_o^{(1)}\right)\right), \tag{15}$$

$$a_4 = \frac{1}{b_2}\left(\left(X_o^{(4)} - Y_o^{(1)}\right)\left(Y_o^{(2)} - X_o^{(1)}\right) - \left(Y_o^{(4)} + X_o^{(1)}\right)\left(X_o^{(2)} + Y_o^{(1)}\right)\right), \tag{16}$$

$$b_4 = \frac{1}{b_2}\left(\left(X_o^{(4)} - Y_o^{(1)}\right)\left(X_o^{(2)} + Y_o^{(1)}\right) + \left(Y_o^{(4)} + X_o^{(1)}\right)\left(Y_o^{(2)} - X_o^{(1)}\right)\right). \tag{17}$$

The invariants are first implemented to find the orientation of the canonical reference frame $\widetilde{\mathcal{F}}$. More specifically, the unit vectors of the $\widetilde{X}-$ and $\widetilde{Y}-$ axis are given by

$$\hat{\widetilde{X}} = \frac{1}{b_2}\begin{Bmatrix} Y_o^{(2)} - X_o^{(1)} \\ Y_o^{(1)} + X_o^{(2)} \end{Bmatrix}; \qquad \hat{\widetilde{Y}} = \frac{1}{b_2}\begin{Bmatrix} X_o^{(2)} + Y_o^{(1)} \\ Y_o^{(2)} - X_o^{(1)} \end{Bmatrix}. \tag{18}$$

Once $\widetilde{\mathcal{F}}$ is determined, the position of the generic point P and its geometric derivatives, with respect to the canonical frame at the instant $\phi = 0$, can be written in terms of the geometric invariants as

$$\widetilde{X}_P = \widetilde{x}, \qquad \widetilde{Y}_P = \widetilde{y} = \widetilde{y}, \tag{19}$$

$$\widetilde{X}_P^{(1)} = -\widetilde{y}, \qquad \widetilde{Y}_P^{(1)} = \widetilde{x}, \tag{20}$$

$$\widetilde{X}_P^{(2)} = -\widetilde{x}, \qquad \widetilde{Y}_P^{(2)} = b_2 - \widetilde{y}, \tag{21}$$

$$\widetilde{X}_P^{(3)} = a_3 + \widetilde{y}, \qquad \widetilde{Y}_P^{(3)} = b_3 - \widetilde{x}, \tag{22}$$

$$\widetilde{X}_P^{(4)} = a_4 + \widetilde{x}, \qquad \widetilde{Y}_P^{(4)} = b_4 + \widetilde{y}. \tag{23}$$

Then, the geometric characteristics of the motion are described in $\widetilde{\mathcal{F}}$ by the following entities:

- curvature,

$$\kappa = \frac{\widetilde{x}^2 + \widetilde{y}^2 - b_2\widetilde{y}}{\left(\widetilde{x}^2 + \widetilde{y}^2\right)^{\frac{3}{2}}}; \tag{24}$$

- center of curvature Ω,

$$\left\{\widetilde{x}_\Omega\,,\,\widetilde{y}_\Omega\right\} \equiv \left\{-\frac{b_2\widetilde{x}\widetilde{y}}{\widetilde{x}^2 + \widetilde{y}^2 - b_2\widetilde{y}}\,,\,-\frac{b_2\widetilde{y}^2}{\widetilde{x}^2 + \widetilde{y}^2 - b_2\widetilde{y}}\right\}; \tag{25}$$

- inflection circle I, from Eq. (24), the locus of the points with zero curvature κ,

$$\widetilde{x}^2 + \widetilde{y}^2 - b_2\widetilde{y} = 0\,; \tag{26}$$

  the point $I \in I$, antipode of P_1, is the inflection pole;
- cubic of stationary curvature, that is the locus of the points with stationary curvature, obtained by imposing equal to zero the derivative of the curvature κ at $\phi = 0$,

$$(\widetilde{y}^2 + \widetilde{x}^2)(a_3\widetilde{x} + b_3\widetilde{y}) + 3\widetilde{x}b_2(\widetilde{x}^2 + \widetilde{y}^2 - b_2\widetilde{y}) = 0\,; \tag{27}$$

- Ball's point, defined as the intersection of the cubic of stationary curvature with the inflection circle (other than the velocity pole),

$$\left\{\widetilde{x}_{Ba}\,,\,\widetilde{y}_{Ba}\right\} \equiv \left\{-b_3\frac{b_2a_3}{a_3^2 + b_3^2}\,,\,a_3\frac{b_2a_3}{a_3^2 + b_3^2}\right\}; \tag{28}$$

- derivative of the cubic of stationary curvature,

$$c_4(\widetilde{y}^2\widetilde{x} + \widetilde{x}^3) + c_1(\widetilde{y}^3 + \widetilde{y}\widetilde{x}^2) + c_5\widetilde{x}^2 + c_6\widetilde{x}\widetilde{y} + c_2\widetilde{y}^2 + c_3\widetilde{y} = 0\,, \tag{29}$$

  where $c_1 = 5b_2 + 4a_3 - b_4$, $c_2 = -4a_3b_2 - 9b_2^2$, $c_3 = 3b_2^3$, $c_4 = -a_4 - 4b_3$, $c_5 = -3b_2^2$, $c_6 = 4b_2b_3$.

Since the Ball's point is obtained as the intersection of Eq. (27) with Eq. (26), its trajectory has four contact points with a straight line for three infinitesimal, subsequent rotations of the moving plane. In addition, the real solutions of the system composed of Eqs. (27) and (29) give the coordinates of the Burmester points, which are points with a trajectory that, for four infinitesimal, subsequent rotations of the moving plane, have five contact points with the osculating circle.

3. Motion description at the element level

According to the formulation presented in Section 2, the instantaneous geometric invariants can be calculated once the coordinates of the point o, origin of the moving frame $\leq$, are defined as functions of the variable ϕ. In case of constant-curvature flexures, with uniform cross-section and subject to end-moment load, the functions

$$X_o = X_o(\phi)\,, \tag{30}$$

$$Y_o = Y_o(\phi)\,, \tag{31}$$

can be obtained in closed form.

With reference to Fig. 2(a), under the Euler-Bernoulli assumptions, the moment-curvature relation can be written as

$$\frac{d\theta}{ds} = \frac{M}{EI}\,, \tag{32}$$

where s is the arc-length coordinate, $d\theta/ds$ is the curvature, M is the internal bending moment, and EI is the bending stiffness. The figure shows the elastic element, in neutral and deflected configurations, and the fixed and moving reference frames. The origin O of the fixed frame $\mathcal{F}\{O, X, Y\}$ is coincident to the anchored end of the beam axis, and the Y-axis is collinear to the axis chord $\overline{OE}$. The mobile frame $\leq\{o, x, y\}$ has origin o coincident to the free-end E of the beam axis. For $\phi = 0$, the frames $\leq$ and $\mathcal{F}$ have the same orientation.

At the generic instant ϕ, the pose of the moving frame with respect to the fixed one can be determined from Eq. (32), by separating variables, using the chain rule of differentiation, and integrating, as [62]

$$\phi = \frac{M}{EI}L, \tag{33}$$

$$X_E = \frac{\sin(\phi)}{\phi}L \tag{34}$$

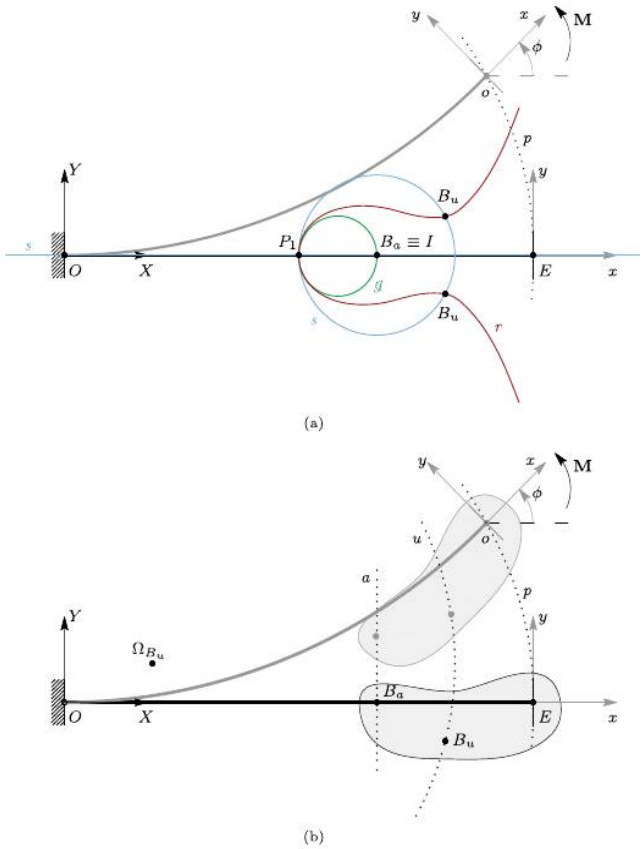

Fig. 2. Straight-axis flexure in neutral (black) and deformed (gray) configurations: geometric description of the motion. (a): instantaneous center of rotation P_1, inflection circle (I), cubic of stationary curvature and its derivative (s and r, respectively) Ball's point (B_a), and Burmester's points (B_u). (b): approximated straight trajectory a of the Ball's point, and approximated circular trajectory u of the Burmester's point with center of curvature Ω_{B_u}.
(For interpretation of the references to color in this figure legend, the reader is referred to the web version of this article.)

$$Y_E = \frac{\cos(\phi) - 1}{\phi} L, \tag{35}$$

where L is the length of the flexure axis. Therefore, according to the notation introduced in Section 2, the non-dimensional functions

$$X_o = \frac{\sin(\phi)}{\phi}, \tag{36}$$

$$Y_o = \frac{1 - \cos(\phi)}{\phi}, \tag{37}$$

define the path p of the free-end section in function of ϕ, and can be used to find the centrodes Eqs. (7) and (9) and the canonical references Eq. (18), and to evaluate Eqs. (13) to (17). Once the geometric invariants are obtained, the geometric entities described in Section 2 can be straightforwardly determined [53].

The results are reported in Fig. 2. More specifically, Fig. 2(a) shows the instantaneous center of rotation, the inflection circle, the cubic of stationary curvature and its derivative, the Ball's and the Burmester's points. If $L = |OE|$ is the length of the beam's axis, P_1 lies on the $X-$axis with abscissa $X_{P_1} = L/2$. The Ball's point B_a lies also on the $X-$axis with abscissa $X_{B_a} = 2L/3$, and it is coincident to the inflection pole I, antipodal of P_1 on the inflection circle. The diameter of the inflection circle is $|P_1 B_a| = L/6$. The coordinates of the Burmester's point are $B_u \equiv (13L/16; -\sqrt{15}L/48)$ with center of curvature $\Omega_{B_u} \equiv (3/16; \sqrt{15}/48)$.

The approximated straight trajectory of the Ball's point, and the approximated circular trajectory of the Burmester's point, with its center of curvature, are shown in Fig. 2(b).

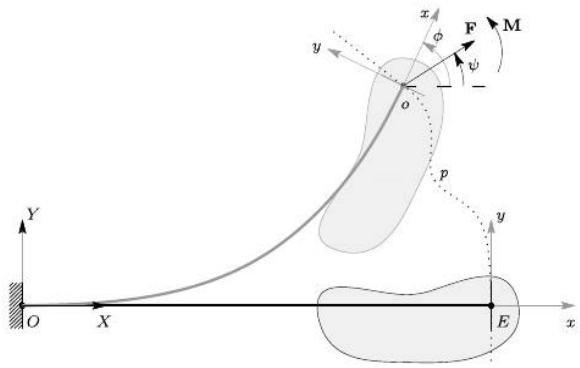

Fig. 3. Straight-axis flexure under a combined load.

It is worth noting that, for uniform flexures under end-moment load, Eq. (33) expresses a direct relation between the moment **M** and the angle ϕ, representing the orientation of the moving frame with respect to the fixed one. The path of the free-end section is defined, and its pose depends only on the value of **M**. Therefore, this case is conservative, and the formulation based on the geometric invariants leads to closed-form expressions.

However, a more general scenario is reported in Fig. 3. The free-end section is subject to a moment **M** and to a force **F** inclined at the angle ψ. The pose of the free-end section is given by [35,62]

$$L = \int_0^{\phi} \frac{d\theta}{\sqrt{\frac{2F}{EI}\left[\cos(\phi-\psi)-\cos(\theta-\psi)\right]+\left(\frac{M}{EI}\right)^2}}, \tag{38}$$

$$x_E = \int_0^{\phi} \frac{\cos\theta\, d\theta}{\sqrt{\frac{2F}{EI}\left[\cos(\phi-\psi)-\cos(\theta-\psi)\right]+\left(\frac{M}{EI}\right)^2}}, \tag{39}$$

$$y_E = \int_0^{\phi} \frac{\sin\theta\, d\theta}{\sqrt{\frac{2F}{EI}\left[\cos(\phi-\psi)-\cos(\theta-\psi)\right]+\left(\frac{M}{EI}\right)^2}}. \tag{40}$$

The solution of Eqs. (38)–(40) is not trivial, since it involves geometric and load parameters. The angle ϕ, unknown in forward problems, appears as the upper limit of the integral and in the radicand. The occurrence of one or more inflection points should also be taken into account. Generally, it is not possible to find closed-form solutions of the system of Eqs. (38)–(40). Several strategies have be considered for the solution, including elliptic integrals, non-linear shooting, Adomian decomposition, integral approaches, hypergeometric functions [14,63–67].

Besides the issue regarding the solution, it is important to note that this case is not conservative, since the path p of the point E depends on **M**, **F**, and ψ, namely, on the loading history. Furthermore, a result in the form of Eqs. (30) and (31), achieved in the conservative case through Eqs. (36) and (37), should be obtained. This problem becomes more challenging at the mechanism level, as explained in the next section.

4. Motion description at the mechanism level

A planar compliant mechanism can be schematically represented by the two-port model depicted in Fig. 4. The body T, that serves as the output port, is connected to the ground through the elastic suspension $\mathcal{M}$.

The application of the actuation or external loads determines the motion of T, that moves describing the path p, according to the loading history. The path is defined by the deflection of the elastic suspension that, in the general case, is composed of series and parallel arrangements of non-uniform flexures. Therefore, the determination of p is not trivial, as mentioned in the previous section considering uniform beams and discussing Eqs. (38)–(40). Further details regarding the nonlinear analysis at the mechanism level can be found in Refs. [17,18].

The objective of this investigation is to develop a synthesis procedure at the output port level. The method exploits the field of displacements of the output port body and defines the body geometry that meets the functional requirements. In this context, the structure of the suspension $\mathcal{M}$, the path p, and the set of poses of T, resulting from a nonlinear analysis step, are the known data of the problem. It is worth noting that, at the mechanism level, the nonlinear analysis provides only the displacement field of the output port. The internal forces associated with such deformation depend on the material properties and on the flexural rigidity of the flexures, which are not specified in the present formulation. For this reason, the synthesis procedure relies exclusively on the

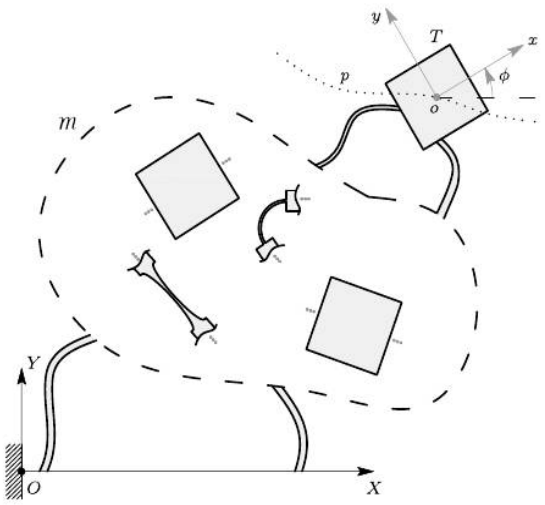

Fig. 4. Two-port model of a compliant mechanism.

kinematic information, namely the path p and the corresponding poses of T. The imposed motion fully characterizes the behaviour of the compliant mechanism for the purposes of the output-port synthesis. The shape of T constitutes the unknown of the problem and is determined through the synthesis procedure detailed in the next section.

5. Synthesis of the output port

The synthesis at the output port level starts from the given compliant mechanism, with defined output port and applied load. The procedure can be summarized as follows.

1. Introduce the fixed frame $\mathcal{F} = \{O, X, Y\}$ to the ground and the moving frame $\leq = \{o, x, y\}$ to the output port body. According to the applied loads, find the relative motion. More specifically, find the poses (position and orientation) of $\leq$ with respect to $\mathcal{F}$. The coordinates $\{X_o, Y_o\}$ define the path p of the origin. Each point of the path is associated to the angle ϕ, that defines the relative orientation of the two frames.
2. From the set of data $\{X_o, Y_o, \phi\}$, find the functions $X_o(\phi)$ and $Y_o(\phi)$. Note that the fourth-order kinematics requires function of class C^4, that is
$$X_o(\phi),\ Y_o(\phi) \in C^4\,. \tag{41}$$
3. Calculate the derivatives
$$X_o^{(1)}, \dots X_o^{(4)}, Y_o^{(1)}, \dots Y_o^{(4)}\,. \tag{42}$$
4. Calculate, according to Eqs. (12) to (17), the geometric invariants
$$a_1,\ b_1,\ \dots a_4,\ b_4.$$
5. Calculate the geometric entities of the motion: the inflection circle Eq. (26), the cubic of stationary curvature Eq. (27) and its derivative Eq. (29), the Ball's point Eq. (28), the Burmester's points (as intersection of the cubic and its derivative) and their center of curvature Eq. (25).
6. Redefine the shape of the output port body in order to include the points of the moving plane that satisfy the design requirements.

In the next section, the synthesis procedure is applied to the synthesis of a compliant four-bar mechanism.

6. Synthesis of the output port of a compliant four-bar mechanism

The assigned compliant mechanism is depicted in Fig. 5. The compliant system incorporates both straight and curved flexure hinges, reflecting some of the possible design choices aimed at satisfying different design requirements, such as predictable rotational behavior, reduced axis drift, or improved stress distribution. Since the proposed synthesis procedure relies solely on the kinematic field generated by the existing compliant suspension, it remains applicable regardless of the specific hinge geometry. The output port T is the coupler, whereas the motion is generated through an applied rotation to the body connected to the frame through a revolute joint in O. The fixed and moving frames, $\mathcal{F}$ and $\leq$, respectively, are represented in the figure.

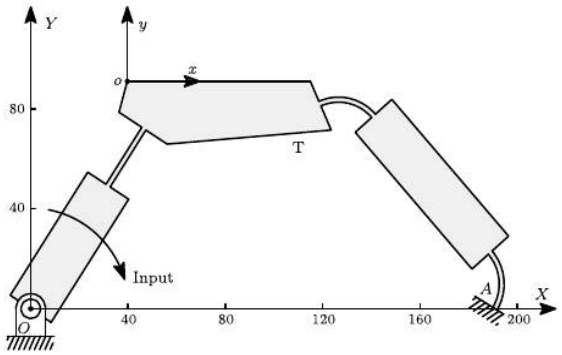

Fig. 5. Compliant mechanism, output port T and motion input.

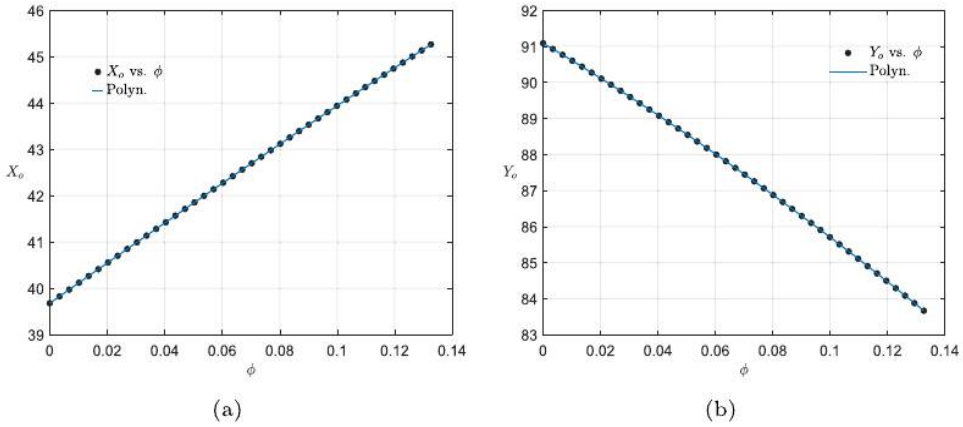

Fig. 6. Data points and fitting of $X_o(\phi)$ (a) and $Y_o(\phi)$ (b).

Finite element simulations are performed with the commercial software Ansys, taking into account geometric nonlinearities. A fixed support has been applied to the cross-section in A. The input motion has been modelled by imposing an increasing rotation, up to 10 deg. A two-dimensional simulation was performed using PLANE182 elements, with local mesh refinement applied in correspondence with the flexible members.

Position and orientation of the moving frame are acquired for each value of the applied displacement through the set of coordinates X_o, Y_o, ϕ.

The functions $X_o(\phi)$ and $Y_o(\phi)$ have been obtained by curve fitting, resorting to the polynomials:

$$X_o(\phi) = p_{x1}\phi^4 + p_{x2}\phi^3 + p_{x3}\phi^2 + p_{x4}\phi + p_{x5}\,, \tag{43}$$

$$Y_o(\phi) = p_{y1}\phi^4 + p_{y2}\phi^3 + p_{y3}\phi^2 + p_{y4}\phi + p_{y5}\,. \tag{44}$$

Fourth-order polynomial fitting is adopted as it provides the simplest analytical representation ensuring C^4 continuity, which is required for evaluating the instantaneous geometric invariants up to fourth order. The data point and the fitting curves are reported in Fig. 6.

From Eqs. (43) and (44) and their derivatives Eq. (42), it is possible to calculate, according to Eqs. (12) to (17), the geometric invariants, and the geometric entities of the motion, according to Eqs. (25) to (29).

The results are reported in Fig. 7, showing the inflection circle, the cubic of the stationary curvature and its derivative, and the Ball's and the Burmester's points.

Once the positions of the points of interest have been obtained, the output port is reshaped accordingly, as shown in Fig. 8. In the illustrative case, the Ball point and two of the four Burmester points (B_{u1} and B_{u4}) are embedded in the redesigned geometry.

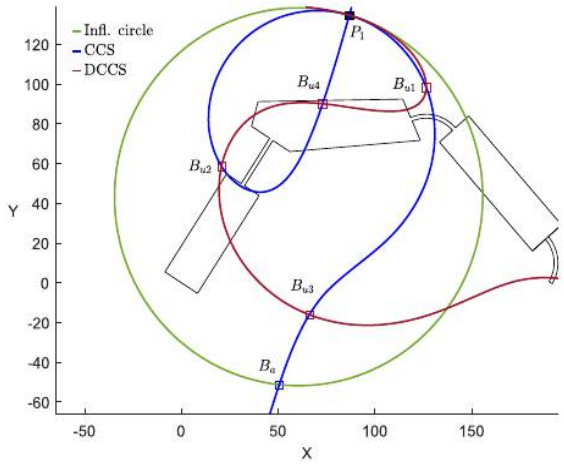

Fig. 7. Inflections circle, cubic of the stationary curvature and its derivative, Ball's and Burmester's points.

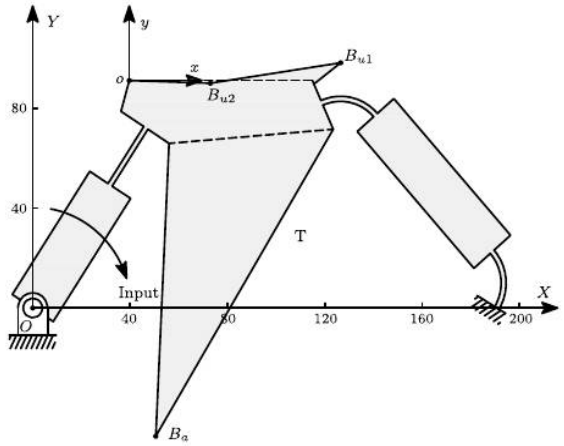

Fig. 8. Reshaping of the output port for the inclusion of the Ball's and Burmester's points. Initial shape shown in dashed lines.

The remaining Burmester points are intentionally omitted to maintain geometric clarity, as incorporating all four would not provide additional insight for the purpose of demonstrating the synthesis procedure.

To validate the synthesis procedure, finite element simulations were performed on the reshaped compliant mechanism, and the corresponding results are presented in Fig. 9. The figure reports the trajectories of the Ball point and of the two selected Burmester points under an input rotation of 20 deg, i.e., twice the rotation prescribed during the determination of these points. This choice allows assessing the effectiveness of the method beyond the range originally employed for the synthesis. The deflected configuration is shown together with the theoretical paths of motion. For the Ball point, the theoretical direction is orthogonal to the direction $P_1 B_a$, whereas the circular paths associated to the Burmester points are obtained from Eq. 24 and 25. A detailed view of the three paths is provided in Fig. 10. For the applied rotation, the discrepancies between the numerical and theoretical trajectories of the Ball's and Burmester's points are negligible.

7. Discussion

In this section, some aspects regarding advantages and limitations of the proposed synthesis procedure are briefly discussed.

The first aspect regards the core of the procedure, based on infinitesimal displacements, and the design of compliant mechanisms, that often requires the design of systems undergoing large deflections. Infinitesimal displacements lead to the definition of

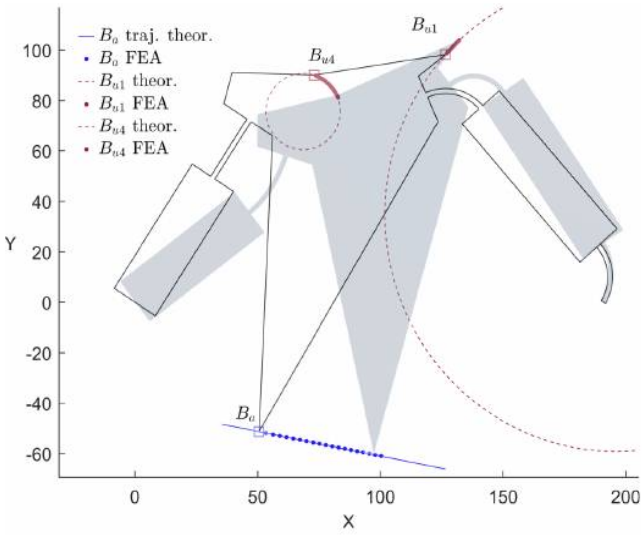

Fig. 9. Compliant mechanism in neutral (contour solid line) and in deflected (cyan) configurations, and numerical and theoretical trajectories of the Ball's and Burmester's points.

an approximate path that follow the target one with accuracy that depends on the kinematic order of the implemented approach. The Ball's and Burmester's points are determined with geometric entities associated to the third and to the fourth order kinematics, respectively. This means that the Ball's point is characterized by a third order contact, or by four infinitesimally separated points in common with the curve to be approximated. On the other hand, the Burmester's point is characterized by a fourth order contact, or by five infinitesimally separated points in common with the curve to be approximated. Generally, high-order kinematics at the infinitesimal level leads to accurate path approximations for finite range of motions. For decades, this feature has been largely exploited in the rigid-body synthesis, and can be exploited in the design of compliant mechanism undergoing moderately large or even large deflections.

The second aspect regards the synthesis procedure operating at the output port level. Starting from an already defined compliant system could be advantageous. In fact, the design of a compliant mechanism, starting from scratch, is generally challenging, considering the inherent coupling of the kinematic and elastomechanical behaviours. On the other hand, the motion of the output port of a compliant mechanism, with assigned actuation law, is already defined. Even if the various geometric entities can be obtained, a feasible solution in terms of Ball's or the Burmester's points is not guaranteed. In fact, these points are points of intersection that could not exist or could not belong to a suitable design region. Furthermore, the reshaping process concerns only the output-port body, leaving the compliant suspension unmodified. As a result, the stiffness characteristics of the mechanism are generally preserved. Minor dynamic variations due to changes in mass distribution can be mitigated by simple design measures, as mass reduction or compensating geometry.

The third aspect concerns the purely kinematic nature of the proposed formulation. The nonlinear analysis required prior to the synthesis provides only the displacement field of the output port, whereas the internal forces depend on parameters that are not specified in this framework. For this reason, the procedure relies only on the kinematic information needed to construct the geometric entities of the Ball's and Burmester's points and to perform the output-port reshaping.

The fouth aspect regards the sensitivity to the design parameters that, in this case, are the position and the orientation of the moving frame associated to the output port. Generally, small variation of these parameters could lead to significant variation of the geometric entities involved in the procedure.

Generally, the complexity of the synthesis problem can be reduced by considering a proper compliant mechanism at the basis of the procedure, for example by resorting to the rigid-body replacement. In this case, the synthesis based on the geometric invariants could improve and optimize the output port motion with respect to the target path.

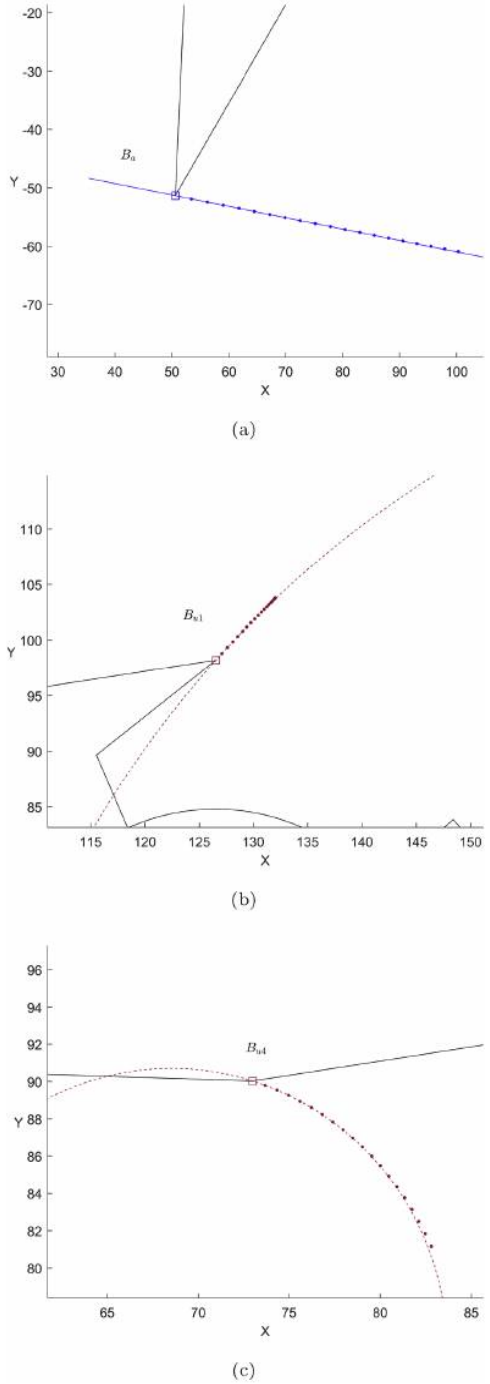

Fig. 10. Details of the paths followed by the Ball's (a) and Burmester's (b) points, for an input rotation of 20 deg. Theoretical and numerical paths in dashed and dotted lines, respectively.

8. Conclusions

In this paper, a procedure for the synthesis of compliant mechanisms at the output port level, based on the instantaneous geometric invariants, has been presented. The method exploits the field of displacements of the output port of a given compliant mechanism to determine the points of the moving plane that satisfy the design requirements. More specifically, the motion is characterized through the inflection circle, the cubic of stationary curvature, and its derivative. These geometric entities lead to the identification of the special points on the plane, that are the Ball's and the Burmester's points, approximating straight paths to the third order, and circular paths to the fourth order, respectively. The procedure has been applied to the synthesis of a compliant four-bar mechanism and the theoretical results have been validated through nonlinear finite element simulations. The advantage of this method lies in its ability to modify an existing compliant mechanism, focusing only on reshaping the output port rather than designing the entire structure from scratch. However, since the motion field is predefined, a feasible solution may not always be available or compatible with specific application requirements. This approach could also be useful as a subsequent design step, enabling the optimization of already designed compliant mechanisms to meet target path specifications.

CRediT authorship contribution statement

M. Verotti: Writing – review & editing, Writing – original draft, Validation, Software, Methodology, Funding acquisition, Formal analysis, Conceptualization.

Data availability

No data was used for the research described in the article.

Declaration of competing interest

The author declares that he have no known competing financial interests or personal relationships that could have appeared to influence the work reported in this paper.

Acknowledgement

This research is funded by the Italian Ministry of University and Research through the PRIN 2022 project "Viscoelastic Characterization of Soft Materials at the Microscale", grant number 2022HM53EA, CUP D53C24004060006 .

References

[1] L. Meng, R. Kang, D. Gan, G. Chen, L. Chen, D.T. Branson, J.S. Dai, A mechanically intelligent crawling robot driven by shape memory alloy and compliant bistable mechanism, J. Mech. Rob. 12 (6) (2020). https://doi.org/10.1115/1.4046837
[2] P. Bilancia, M. Baggetta, G. Berselli, L. Bruzzone, P. Fanghella, Design of a bio-inspired contact-aided compliant wrist, Rob. Comput. Integr. Manuf. 67 (2021) 102028. https://doi.org/10.1016/j.rcim.2020.102028
[3] P. Kuresangsai, M.O.T. Cole, G. Hao, Analysis and design optimization of a compliant robotic gripper mechanism with inverted flexure joints, Mech. Mach. Theory 202 (2024) 105779. https://doi.org/10.1016/j.mechmachtheory.2024.105779
[4] Y. Tian, D. Zhang, B. Shirinzadeh, Dynamic modelling of a flexure-based mechanism for ultra-precision grinding operation, Precis. Eng. 35 (4) (2011) 554–565. https://doi.org/10.1016/j.precisioneng.2011.03.001
[5] T. Wang, Y. Li, Y. Zhang, R. Lin, J. Qian, Z. Dou, Design of a flexure-based parallel XY micropositioning stage with millimeter workspace and high bandwidth, Sens. Actuators A 331 (2021) 112899. https://doi.org/10.1016/j.sna.2021.112899
[6] M. Horvatek, Improved linear stage hinge design suitable for additive manufacturing, J. Mech. Sci. Technol. 37 (3) (2023) 1139–1144. https://doi.org/10.1007/s12206-022-2111-5
[7] W. Zeng, F. Gao, H. Jiang, C. Huang, J. Liu, H. Li, Design and analysis of a compliant variable-diameter mechanism used in variable-diameter wheels for lunar rover, Mech. Mach. Theory 125 (2018) 240–258. https://doi.org/10.1016/j.mechmachtheory.2018.03.003
[8] C.A. Gebara, P.D. Lytal, J.J. Rimoli, Additive manufacturing of compliant mechanisms for deployable aerospace structures, J. Mater. Eng. Perform. 31 (8) (2022) 6083–6091. https://doi.org/10.1007/s11665-022-07050-6
[9] D. Budzyń, H. Zare-Behtash, A. Cowley, A. Cammarano, Implicit lunar dust mitigation technology: compliant mechanisms, Acta Astronaut. 203 (2023) 146–156. https://doi.org/10.1016/j.actaastro.2022.11.042
[10] G. Hao, J. Zhu, Design of a monolithic double-slider based compliant gripper with large displacement and anti-buckling ability, Micromachines 10 (10) (2019). https://doi.org/10.3390/mi10100665
[11] P. Schmitt, M. Hoffmann, A force-compensated compliant MEMS-amplifier with electrostatic anti-springs, Microsyst. Nanoeng. 9 (83) (2023). https://doi.org/10.1038/s41378-023-00557-5
[12] A. Buzzin, L. Giannini, G. Bocchetta, A. Notargiacomo, E. Giovine, A. Scorza, R. Asquini, G. de Cesare, N.P. Belfiore, On the dependency of the electromechanical response of rotary MEMS/NEMS on their embedded flexure hinges' geometry, Micromachines 14 (12) (2023). https://doi.org/10.3390/mi14122229
[13] A. Cammarata, P.D. Maddìo, R. Sinatra, N.P. Belfiore, Direct kinetostatic analysis of a gripper with curved flexures, Micromachines 13 (12) (2022). https://doi.org/10.3390/mi13122172
[14] L. Chen, An integral approach for large deflection cantilever beams, Int. J. Non Linear Mech. 45 (3) (2010) 301–305.
[15] M. Batista, Large deflections of shear-deformable cantilever beam subject to a tip follower force, Int. J. Mech. Sci. 75 (2013) 388–395. https://doi.org/10.1016/j.ijmecsci.2013.08.006
[16] A. Mukherjee, S.F. Ali, A. Arockiarajan, Compliant structure under follower forces and any combined loading: theoretical and experimental studies, Int. J. Mech. Sci. 153-154 (2019) 75–82. https://doi.org/10.1016/j.ijmecsci.2019.01.016
[17] G. Hao, J. Yu, H. Li, A brief review on nonlinear modeling methods and applications of compliant mechanisms, Front. Mech. Eng. 11 (2) (2016) 119–128. https://doi.org/10.1007/s11465-016-0387-9

[18] M. Ling, L.L. Howell, J. Cao, G. Chen, Kinetostatic and dynamic modeling of flexure-based compliant mechanisms: a survey, Appl. Mech. Rev. 72 (3) (2020) 030802. https://doi.org/10.1115/1.4045679

[19] P. Bilancia, G. Berselli, An overview of procedures and tools for designing nonstandard beam-based compliant mechanisms, Comput. Aided Des. 134 (2021) 103001. https://doi.org/10.1016/j.cad.2021.103001

[20] J.A. Gallego, J. Herder, Synthesis methods in compliant mechanisms: an overview, in: Volume 7: 33rd Mechanisms and Robotics Conference, Parts A and B, IDETC-CIE2009, ASMEDC, 2009. https://doi.org/10.1115/detc2009-86845

[21] Handbook of Compliant Mechanisms, Wiley, 2013.

[22] O. Sorgonà, O. Giannini, M. Verotti, Projective synthesis of planar compliant mechanisms, Mech. Mach. Theory 210 (2025). https://doi.org/10.1016/j.mechmachtheory.2025.106010

[23] O. Sorgonà, O. Giannini, M. Verotti, Single-point synthesis of compliant mechanisms, Precis. Eng. 93 (2025) 58–69. https://doi.org/10.1016/j.precisioneng.2024.12.012

[24] O. Sorgonà, L.E. Bruzzone, O. Giannini, M. Verotti, Isotropic point synthesis of flexures and of compliant mechanisms, Precis. Eng. 97 (2026) 624–631. All Open Access; Hybrid Gold Open Access, https://doi.org/10.1016/j.precisioneng.2025.09.027

[25] L. Cao, A.T. Dolovich, A. Chen, W. Zhang, Topology optimization of efficient and strong hybrid compliant mechanisms using a mixed mesh of beams and flexure hinges with strength control, Mech. Mach. Theory 121 (2018) 213–227. https://doi.org/10.1016/j.mechmachtheory.2017.10.022

[26] B. Zhu, X. Zhang, H. Zhang, J. Liang, H. Zang, H. Li, R. Wang, Design of compliant mechanisms using continuum topology optimization: a review, Mech. Mach. Theory 143 (2020) 103622. https://doi.org/10.1016/j.mechmachtheory.2019.103622

[27] B. Niu, X. Liu, M. Wallin, E. Wadbro, Topology optimization of compliant mechanisms considering strain variance, Struct. Multidiscip. Optim. 62 (3) (2020) 1457–1471. https://doi.org/10.1007/s00158-020-02632-1

[28] S. Xia, N. Wang, B. Chen, X. Zhang, W. Chen, Topology optimization of compliant mechanisms including links, supports and material distribution, Comput. Struct. 291 (2024) 107210. https://doi.org/10.1016/j.compstruc.2023.107210

[29] Z.-Q. Zhang, M.-Q. Niu, L.-Q. Chen, Analysis and optimization of a quasi-zero-stiffness vibration isolator based on partially rigidized compliant mechanisms, Eng. Struct. 343 (2025) 121048. https://doi.org/10.1016/j.engstruct.2025.121048

[30] A. Saxena, A contact-aided compliant displacement-delimited gripper manipulator, J. Mech. Rob. 5 (4) (2013). https://doi.org/10.1115/1.4024728

[31] P. Kumar, R.A. Sauer, A. Saxena, On topology optimization of large deformation contact-aided shape morphing compliant mechanisms, Mech. Mach. Theory 156 (2021) 104135. https://doi.org/10.1016/j.mechmachtheory.2020.104135

[32] A.K. Rai, A. Saxena, N.D. Mankame, Unified synthesis of compact planar path-generating linkages with rigid and deformable members, Struct. Multidiscip. Optim. 41 (6) (2009) 863–879. https://doi.org/10.1007/s00158-009-0458-1

[33] J. Reinisch, E. Wehrle, J. Achleitner, Multiresolution topology optimization of large-deformation path-generation compliant mechanisms with stress constraints, Appl. Sci. 11 (6) (2021) 2479. https://doi.org/10.3390/app11062479

[34] L. Zhang, S. Koppen, F. van Keulen, Connectivity-driven topology optimization for path-following compliant mechanism: a formulation with predictive volume constraints and adaptive strategies for gray element suppression, Struct. Multidiscip. Optim. 68 (2) (2025). https://doi.org/10.1007/s00158-025-03962-8

[35] H.-J. Su, A pseudorigid-body 3R model for determining large deflection of cantilever beams subject to tip loads, J. Mech. Rob. 1 (2) (2009) 021008. https://doi.org/10.1115/1.3046148

[36] Y.-Q. Yu, S.-K. Zhu, 5R pseudo-rigid-body model for inflection beams in compliant mechanisms, Mech. Mach. Theory 116 (2017) 501–512. https://doi.org/10.1016/j.mechmachtheory.2017.06.016

[37] P.P. Valentini, E. Pennestrì, Second-order approximation pseudo-rigid model of leaf flexure hinge, Mech. Mach. Theory 116 (2017) 352–359. https://doi.org/10.1016/j.mechmachtheory.2017.06.007

[38] M. Verotti, A pseudo-rigid body model based on finite displacements and strain energy, Mech. Mach. Theory 149 (2020) 103811. https://doi.org/10.1016/j.mechmachtheory.2020.103811

[39] J.B. Hopkins, M.L. Culpepper, Synthesis of multi-degree of freedom, parallel flexure system concepts via freedom and constraint topology (FACT) - Part I: principles, Precis. Eng. 34 (2) (2010) 259–270. https://doi.org/10.1016/j.precisioneng.2009.06.008

[40] J.B. Hopkins, M.L. Culpepper, Synthesis of multi-degree of freedom, parallel flexure system concepts via freedom and constraint topology (FACT). Part II: practice, Precis. Eng. 34 (2) (2010) 271–278. https://doi.org/10.1016/j.precisioneng.2009.06.007

[41] J.B. Hopkins, J. Rivera, C. Kim, G. Krishnan, Synthesis and analysis of soft parallel robots comprised of active constraints, J. Mech. Rob. 7 (1) (2015). https://doi.org/10.1115/1.4029324

[42] N.C. Archer, J.B. Hopkins, Analysis and synthesis of interconnected hybrid mechanisms using freedom and constraint topologies (FACT), Mech. Mach. Theory 200 (2024) 105722. https://doi.org/10.1016/j.mechmachtheory.2024.105722

[43] N.C. Archer, J.B. Hopkins, Large-range rotation-to-translation compliant transmission mechanism, J. Mech. Des. 145 (12) (2023). https://doi.org/10.1115/1.4063160

[44] C.J. Kim, S. Kota, Y.-M. Moon, An instant center approach toward the conceptual design of compliant mechanisms, J. Mech. Des. 128 (3) (2005) 542–550. https://doi.org/10.1115/1.2181992

[45] C.J. Kim, Y.-M. Moon, S. Kota, A building block approach to the conceptual synthesis of compliant mechanisms utilizing compliance and stiffness ellipsoids, J. Mech. Des. 130 (2) (2008). https://doi.org/10.1115/1.2821387

[46] C.J. Kim, On the geometry of stiffness and compliance under concatenation, J. Mech. Rob. 12 (2) (2020). https://doi.org/10.1115/1.4046048

[47] C. Li, S.-C. Chen, Design of compliant mechanisms based on compliant building elements. Part I: principles, Precis. Eng. 81 (2023) 207–220. https://doi.org/10.1016/j.precisioneng.2023.01.006

[48] O. Sorgonà, N.P. Belfiore, O. Giannini, M. Verotti, Application of the ellipse of elasticity theory to the functional analysis of planar compliant mechanisms, Mech. Mach. Theory 184 (2023) 105308. https://doi.org/10.1016/j.mechmachtheory.2023.105308

[49] O. Sorgonà, S. Serafino, O. Giannini, M. Verotti, Analysis of compliant mechanisms with series and parallel substructures through the ellipse of elasticity theory, Int. J. Solids Struct. 298 (2024) 112847. https://doi.org/10.1016/j.ijsolstr.2024.112847

[50] P.P. Valentini, M. Cirelli, E. Pennestrì, Second-order approximation pseudo-rigid model of flexure hinge with parabolic variable thickness, Mech. Mach. Theory 136 (2019) 178–189. https://doi.org/10.1016/j.mechmachtheory.2019.03.006

[51] M. Cera, M. Cirelli, L. Colaiacovo, P.P. Valentini, Second-order approximation pseudo-rigid model of circular arc flexure hinge, Mech. Mach. Theory 175 (2022) 104963. https://doi.org/10.1016/j.mechmachtheory.2022.104963

[52] C. Iandiorio, P. Salvini, Elasto-kinematics and instantaneous invariants of compliant mechanisms based on flexure hinges, Micromachines 14 (4) (2023) 783. https://doi.org/10.3390/mi14040783

[53] M. Verotti, High-order kinematics of uniform flexures, Mech. Mach. Theory 196 (2024) 105631. https://doi.org/10.1016/j.mechmachtheory.2024.105631

[54] M. Krause, Analysis der Ebenen Bewegung, Walter de Gruyter GmbH & Co KG, 2021.

[55] G.R. Veldkamp, Canonical systems and instantaneous invariants in spatial kinematics, J. Mech. 2 (3) (1967) 329–388. https://doi.org/10.1016/0022-2569(67)90006-7

[56] O. Bottema, B. Roth, Theoretical Kinematics, 24, Courier Corporation, 1990.

[57] A. Inalcik, S. Ersoy, H. Stachel, On instantaneous invariants of hyperbolic planes, Math. Mech. Solids 22 (5) (2015) 1047–1057. https://doi.org/10.1177/1081286515616283

[58] E. Pennestrì, N.P. Belfiore, On the numerical computation of generalized Burmester points, Meccanica 30 (2) (1995) 147–153. https://doi.org/10.1007/bf00990453

[59] M. Cera, E. Pennestrì, Generalized Burmester points computation by means of Bottema's instantaneous invariants and intrinsic geometry, Mech. Mach. Theory 129 (2018) 316–335. https://doi.org/10.1016/j.mechmachtheory.2018.07.011

[60] C. Lanni, G. Figliolini, L. Tomassi, First and Second Order Centrodes of Slider-Crank Mechanisms by Using Instantaneous Invariants, Springer International Publishing, 2022, pp. 303–310. https://doi.org/10.1007/978-3-031-08140-8_33
[61] C. Lanni, G. Figliolini, L. Tomassi, Higher-order centrodes and Bresse's circles of slider-crank mechanisms, in: Volume 8: 47th Mechanisms and Robotics Conference (MR), IDETC-CIE2023, American Society of Mechanical Engineers, 2023. https://doi.org/10.1115/detc2023-116627
[62] L.L. Howell, Compliant Mechanisms, Wiley, New York, New York, 2001.
[63] L.L. Howell, A. Midha, Parametric deflection approximations for end-loaded, large-deflection beams in compliant mechanisms, J. Mech. Des. 117 (1) (1995) 156–165. https://doi.org/10.1115/1.2826101
[64] C. Kimball, L.W. Tsai, Modeling of flexural beams subjected to arbitrary end loads, J. Mech. Des. Trans. 124 (2) (2002) 223–235. https://doi.org/10.1115/1.1455031
[65] A. Banerjee, B. Bhattacharya, A.K. Mallik, Large deflection of cantilever beams with geometric non-linearity: analytical and numerical approaches, Int. J. Non Linear Mech. 43 (5) (2008) 366–376. https://doi.org/10.1016/j.ijnonlinmec.2007.12.020
[66] A. Cammarata, M. Lacagnina, G. Sequenzia, Alternative elliptic integral solution to the beam deflection equations for the design of compliant mechanisms, Int. J. Interact. Des. Manuf. 13 (2) (2018) 499–505. https://doi.org/10.1007/s12008-018-0512-6
[67] C. Iandiorio, P. Salvini, Large displacements of slender beams in plane: analytical solution by means of a new hypergeometric function, Int. J. Solids Struct. 185-186 (2020) 467–484. https://doi.org/10.1016/j.ijsolstr.2019.09.006